KINETIC STUDIES OF THE GROUND STATE LEAD ATOMS $Pb(6^3P_0)$ GENERATED BY PULSED IRRADIATION AND MONITORED BY TIME-RESOLVED FLUORESCENCE AT λ = 405.78 nm ($Pb(7^3P_1) \rightarrow Pb(6^3P_2)$) FOLLOWING OPTICAL EXCITATION AT λ = 283.31 nm ($Pb(7^3P_1) \leftarrow Pb(6^3P_0)$)

CHARLES F. BELL and DAVID HUSAIN

Department of Physical Chemistry, University of Cambridge, Lensfield Road, Cambridge CB2 1EP (Gt. Britain)

(Received June 2, 1984; in revised form July 25, 1984)

Summary

We describe the first kinetic study of ground state lead atoms by time-resolved atomic fluorescence spectroscopy. $Pb(6^3P_0)$ was generated by the pulsed irradiation of $Pb(CH_3)_4$ in the presence of helium using a high intensity magnetically pinched Garton–Wheaton light source. The transient atom was monitored in the time-resolved mode by off-resonance (direct-line) fluorescence at λ = 405.78 nm ($Pb(7^3P_1) \rightarrow Pb(6^3P_2)$) following resonance excitation at λ = 283.31 nm ($Pb(7^3P_1) \leftarrow Pb(6^3P_0)$). The construction of an intense resonance source for atomic lead involved further application of the microwave-powered cavity originally developed in the Philips Laboratories at Eindhoven which was constructed in these laboratories and used earlier for the kinetic study of atomic bismuth. The photoelectric signals were recorded in the "single-shot" mode using pretrigger photomultiplier gating and were analysed in digital form by computer. The kinetic study included an investigation of the diffusion of $Pb(6^3P_0)$ in helium together with the third-order reactions with oxygen and NO (plus helium) for which we report the following absolute rate constants (300 K):

$k(Pb + O_2 + He) = (2.5 \pm 0.2) \times 10^{-32}$ cm^6 molecules^{-2} s^{-1}

$k(Pb + NO + He) = (9 \pm 3) \times 10^{-31}$ cm^6 molecules^{-2} s^{-1}

These are compared with previous estimates reported from time-resolved atomic resonance absorption measurements on $Pb(6^3P_0)$. Finally, we report fluorescence quenching cross sections for $Pb(7^3P_1)$ of $\sigma_{NO}{}^2 = 38 \pm 3$ Å^2 and $\sigma_{O_2}{}^2 = 12 \pm 8$ Å^2, which are in agreement with data reported earlier from atomic emission measurements on flames.

1. Introduction

Whilst the collisional behaviour of the group IV ground state lead atom $Pb(6p^2(^3P_0))$ has been widely investigated by time-resolved atomic resonance

0047-2670/85/$3.30

absorption spectroscopy following the generation of these atoms by pulsed irradiation [1 - 6], analogous kinetic studies using time-resolved atomic fluorescence for monitoring the transient atoms have not been reported. This is in marked contrast, for example, with the ground state Bi($6p^3(^4S_{3/2})$) of the heavy group V element bismuth which has been the object of kinetic investigations by means of both time-resolved resonance absorption [7] and resonance fluorescence [8 - 11]. Indeed, similar considerations apply to the investigation of the $(np)^2$, $^3P_0$ ground states of other group IV elements which have been studied by means of time-resolved resonance absorption spectroscopy [12], whereas the group V ground states $(np)^3$, $^4S_{3/2}$ have been monitored by both time-resolved resonance absorption and resonance fluorescence [13]; however, a detailed consideration of this wide area of atomic kinetics is too large for discussion here.

Apart from developments in experimental technique, investigation of atomic kinetics by means of these two complementary methods provides information for data analyses arising from the effects of atomic line shapes. In time-resolved resonance absorption measurements, departures from the standard Beer–Lambert law are conveniently expressed over a limited concentration range in terms of the relation [14]

$$I_{tr} = I_0 \exp\{-(\epsilon c l)^\gamma\} \quad (1)$$

where the symbols have their usual significance. There are empirical techniques for determining γ in time-resolved measurements [14]. In some instances, as in the cases for example of Pb(6^3P_0) and Sn(5^3P_0), the γ values for the resonance transitions at λ = 283.31 nm (Pb(7^3P_1) ← Pb(6^3P_0)) and λ = 286.33 nm (Sn(6^3P_1) ← Sn(5^3P_0)) respectively can be determined from "curve-of-growth" measurements [15] on atomic vapours in equilibrium with their solids at elevated temperatures [6, 16]. Kinetic data derived from time-resolved resonance fluorescence measurements depend only upon the functional relationship between fluorescence and particle density, and experimental conditions are normally chosen in which this relationship is sensibly linear, even if there may be significant radiation trapping. It can thus be shown on this basis that the rate constants derived from atomic absorption and fluorescence measurements are connected by the relation [7, 8]

$$\frac{k_{abs}}{k_{fluor}} = \gamma \quad (2)$$

Time-resolved atomic fluorescence measurements on Pb(6^3P_0) in the "single-shot" mode, *i.e.* using single-pulsed irradiation without signal averaging, have not been forthcoming for reasons that are more technical than fundamental. This is because of (a) the failure to generate large densities of Pb(6^3P_0) photochemically from a suitable gaseous precursor using a conventional pulsed light source as opposed to, say, an excimer laser, and (b) the recognition that conventional atomic resonance sources connecting with Pb(6^3P_0) are relatively weak compared with those for many other ground state atoms [3]. Both these limitations have been overcome sufficiently in

the present investigation: (a) a high intensity magnetically pinched Garton–Wheaton flash lamp was used as the source of actinic radiation [17]; (b) we describe a further extension [9] of the use of the microwave-powered cavity reported by Beenakker [18, 19] and Beenakker and Boumans [20] for developing a resonance source at $\lambda = 283.31$ nm ($Pb(7^3P_1) \rightarrow Pb(6^3P_0)$) sufficiently intense for optical excitation for time-resolved monitoring of $Pb(6^3P_0)$ off resonance (direct line) at $\lambda = 405.78$ nm ($Pb(7^3P_1) \rightarrow Pb(6^3P_2) + h\nu$). The first kinetic study of $Pb(6^3P_0)$ by time-resolved atomic fluorescence is described in this paper which also includes the effects of diffusion and the third-order reactions $Pb + O_2 + He$ and $Pb + NO + He$. The kinetic results are compared with those derived from previous measurements using time-resolved resonance absorption. Calculations are presented on the relationship between the fluorescence intensity and the particle density for the transitions at $\lambda = 283.31$ nm and $\lambda = 405.78$ nm in both the presence and absence of radiation trapping. Total line shapes based on the summation of Voigt profiles [15] over the various nuclear hyperfine components are used.

2. Experimental details

The combination of the photochemical reactor and the pulsed irradiation source for time-resolved atomic fluorescence measurements on $Pb(6^3P_0)$ is similar to that employed hitherto for kinetic studies of $Sb(5^4S_{3/2})$ reported by Husain *et al.* [21] with minor modifications. The major modifications were the optical excitation system and the detection system (see later). Unlike previous measurements on $Sb(5^4S_{3/2})$ [21], the high intensity magnetically pinched Garton–Wheaton source [17] (Chelsea Instruments) used for the photochemical generation of atomic lead was employed, not by means of high voltage switching effected through the use of an ignitron [12], but in the conventional manner by the direct application of a voltage difference on charging of 10 kV across the lamp (10 kV; $C = 10\ \mu F$; $E = 500$ J) at a pressure of about 5 mTorr (1 Torr = 133 Pa). Discharge was then initiated using a 30 kV pulse derived from a high voltage transformer. The Garton–Wheaton lamp was optically coupled to the reactor by means of a cleaved LiF disc, in theory giving rise to photolysis at $\lambda > 110$ nm, but this disc required regular cleaning because of deposits from the discharge and eventual replacement on account of the formation of colour centres. A diagram of the machined reactor with a Cassegrain mirror for greater light gathering of the fluorescence signal [21] was given in our earlier paper on time-resolved resonance fluorescence studies of $Bi(6^4S_{3/2})$ [9].

Development of an intense lead emission source for operating at $\lambda = 283.31$ nm ($Pb(7^3P_1) \rightarrow Pb(6^3P_0)$) [22], which is fundamentally a strong transition ($\tau_e(Pb(7^3P_1)) = 5.75 \pm 0.2$ ns [23] and 6.05 ± 0.3 ns [24]), was critical to the construction of a system for monitoring $Pb(6^3P_0)$ in the time-resolved mode. This employed the cylindrical microwave cavity described in our earlier papers [9 - 11] following the design of Beenakker and coworkers

[18 - 20] coupled, in this instance, through a sealed quartz capsule of external diameter approximately 6 mm into which PbI_2 had been sublimed following a number of fractional sublimations and to which krypton gas was added (about 10 Torr) (an EMS Microtron 200 mark 2 was used under the following conditions: 2450 MHz, power at about 55 W; reflected power, about 7 W). This device was difficult to operate over long periods, and it was necessary to heat the capsule with a flame before electrically striking the cavity and to use air cooling once the lamp was operating. Nevertheless, of the various types of atomic lead emission sources tried (including a high intensity hollow cathode source operating at about 100 mA), this was the only one sufficiently intense for time-resolved fluorescence studies of $Pb(6^3P_0)$.

A further important detail in these investigations is the study of the emission from the optically excited $Pb(7^3P_1)$ at $\lambda = 405.78$ nm ($Pb(7^3P_1) \rightarrow Pb(6^3P_2)$) [22]. This enjoys the twofold advantage of reducing the effect of low wavelength scattered light from the Garton–Wheaton pulsed source and reducing steady scattered light, *i.e.* θ_1 (see later), from the atomic excitation source. The standard orthogonal arrangement for time-resolved fluorescence following pulsed irradiation was employed [9]. The transition at $\lambda = 405.78$ nm ($f = 0.14$ [23, 24]) was optically isolated by means of a broad band interference filter (Barr and Stroud MD6 which has a transmission of about 31% at $\lambda = 405.78$ nm and a bandwidth of 18 nm). The transient photoelectric signals at this wavelength were monitored using a photomultiplier tube (EMI 9186B) with a Pyrex end window (900 V, Brandenburg power supply 415 R), thus further eliminating intense UV scattered light from the Garton–Wheaton source. Unlike the procedure adopted in our measurements on $Bi(6^4S_{3/2})$ [9 - 11], the photomultiplier tube was gated in the "pretrigger" mode using circuitry described generally by Husain and Schifino [25] and modifying the circuit given in detail by Acuna *et al.* [26]. Thus, in this particular application, a pulse from a standard delay circuit normally used for conventional kinetic spectroscopy was used to trigger a monostable pulse generator powered by means of an 18 V d.c. stabilized power supply. This gating circuit [25, 26] provided a pulse of magnitude about 100 V and, in this instance, of duration 264 μs across the fifth and seventh dynodes of the photomultiplier tube, thus effectively rendering it insensitive to radiation for this period. A second pulse from the delay circuit, 13 μs subsequent to gating the photomultiplier tube, was then transmitted to the pulse transformer for firing the Garton–Wheaton source. Thus the photomultiplier was "switched on" 251 μs after the intense pulse from the flash lamp.

The photochemical precursor of $Pb(6^3P_0)$ in these measurements was $Pb(CH_3)_4$ rather than $Pb(C_2H_5)_4$ which was used in all earlier investigations [1 - 6] on account of its higher vapour pressure [27]. $Pb(CH_3)_4$ is more convenient in the present application and is considered quantitatively in detail later in terms of the photochemical yield of $Pb(6^3P_0)$. It was subjected to pulsed irradiation in the presence of excess helium buffer gas and the appropriate added reactant. Following the pretrigger photomultiplier gating procedure, the photoelectric signals representing decays at $\lambda = 405.78$ nm,

in turn representing the decay of $Pb(6^3P_0)$, were amplified by means of a current-to-voltage converter to avoid signal distortion [28]. The signals were transferred to a transient recorder (Data Laboratories DL 905) where they were digitized, stored, displayed on an oscilloscope for visual inspection and punched onto paper tape (Datadynamics punch 1133) for subsequent processing in the University of Cambridge IBM 3081 computer. Apart from $Pb(CH_3)_4$ (Associated Octel Co.) and PbI_2 (BDH), all materials (helium, krypton, oxygen and NO) were essentially prepared as described previously [9 - 11].

3. Results and discussion

3.1. Photochemical generation of $Pb(6^3P_0)$ for time-resolved atomic fluorescence monitoring

The requirements for the pulsed generation of transient atoms, in this instance $Pb(6^3P_0)$, in concentrations sufficiently large for time-resolved atomic fluorescence monitoring can conveniently be considered initially by comparison with experimental measurements employing time-resolved atomic resonance absorption spectroscopy [1 - 6]. For absorption measurements photochemical generation is effectively homogeneous along the length of a relatively narrow reactor, and the dimensions of the reaction vessel are essentially defined by its geometry, particularly as far as the path length through which atomic resonance absorption is carried out. In fluorescence measurements the effective size of the reactor is the small volume resulting from the overlap of the cones of radiation from the pulsed initiation source and the resonance source, complicated further by the light collection system. Thus the actinic radiation from the pulsed source is attenuated by the gaseous photochemical precursor in the light path between the LiF optical window coupling the light source to the reactor and the face of the reaction volume. In our earlier papers [9, 10] the rate of production of $Bi(6^4S_{3/2})$ was treated in a simplified form:

$$I_{abs} = I_0 \exp(-\epsilon c l')\epsilon c l \tag{3}$$

where c is the concentration of the photochemical precursor $Bi(CH_3)_3$, ϵ is the maximum extinction coefficient of $Bi(CH_3)_3$, $l' = 6$ cm and l is the effective length of the reaction volume ($l \ll l'$). Following Christie and Porter [28] I_0 was taken to be the intensity of the light output from a conventional flash lamp characterized as a black-body radiator of temperature 6773 K. This was subsequently developed more quantitatively using the form [11]

$$I_{abs} = \int I_\lambda \exp\{-\epsilon(\lambda)cl'\}[1 - \exp\{-\epsilon(\lambda)cl\}]\, d\lambda \tag{4}$$

where I_λ included the wavelength distribution for a black-body radiator with the appropriate correction to account for the area of the incident radiation.

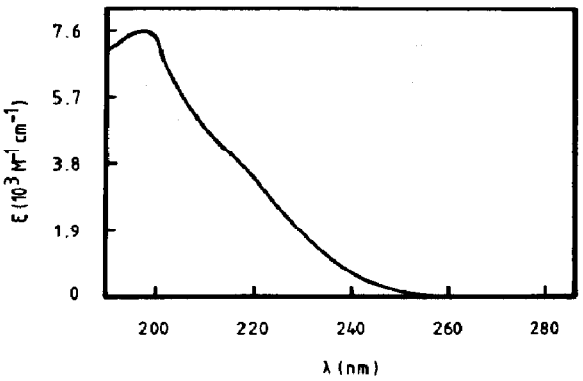

Fig. 1. Variation of the extinction coefficient of gaseous $Pb(CH_3)_4$ with wavelength in the far UV.

In the present measurements the rate of production of $Pb(6^3P_0)$ is calculated by means of eqn. (4) using the measured UV extinction coefficient of $Pb(CH_3)_4$ recorded here (Fig. 1) and approximated to the functional form [11]

$$\epsilon(\lambda) = \epsilon_{max} \exp\{\pm\xi(\lambda - \lambda_{max})\}$$

together with I_λ for black-body radiators at (a) $T = 6773$ K [28] for comparison with the earlier system used for $Bi(6^4S_{3/2})$ [11] and (b) $T = 22\,273$ K. The choice of this latter temperature is determined by the commercially published emission characteristics for the Garton–Wheaton source (Chelsea Instruments), crudely estimated for a black-body of temperature $T = 29\,000$ K using the overall shape of the curve. The wavelength for maximum emission ($\lambda \approx 130$ nm) would correspond approximately to 22 273 K and is employed here to ensure a conservative estimate. The result for the photochemical production of $Pb(6^3P_0)$ is shown in Fig. 2 as a function of $[Pb(CH_3)_4]$. The Garton–Wheaton source is seen to give rise to light absorption, and hence $Pb(6^3P_0)$, a factor of 10^2 greater than that obtained with the conventional flash source for $T = 6773$ K.

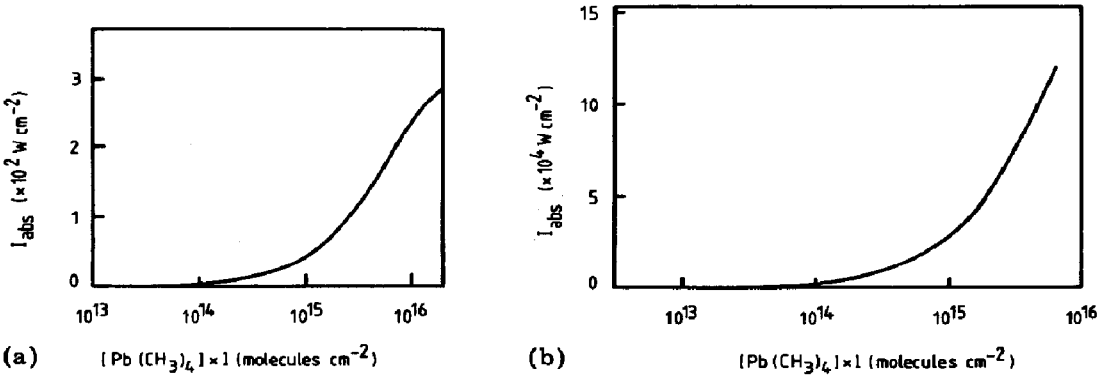

Fig. 2. Intensity of light absorption I_{abs} (W cm^{-2}) by gaseous $Pb(CH_3)_4$ owing to the attenuation of actinic radiation from a black-body radiator for (a) $T = 6773$ K and (b) $T = 22\,273$ K.

3.2. Time-resolved atomic fluorescence for monitoring Pb(6^3P_0)

Prediction of the relationship between the fluorescence intensity and [Pb(6^3P_0)] involves complex computer calculations on radiation trapping of the type we have previously described for Bi($6^4S_{3/2}$) [11]. Whilst it is not our intention to present as much detail here for the case of atomic lead, the conclusions of such calculations are given to illustrate the considerable advantage of carrying out measurements by direct-line fluorescence at λ = 405.78 nm (Pb(7^3P_1) → Pb(6^3P_2)) rather than by employing the resonance transition at λ = 283.31 nm (Pb(7^3P_1) → Pb(6^3P_0)). Figure 3 shows the computer simulation of the line shapes of the two transitions which was obtained by summing the Voigt profiles over the appropriate nuclear hyperfine components. The isotopic abundances were taken from Gordy *et al.* [29] and the mean radiative lifetime τ_e(Pb(7^3P_1) = (5.8 ± 0.2) ns used to calculate the oscillator strengths f for each transition was the average of the two sets of data reported by Saloman and Harper [23] and Cunningham and Link [24]. The nuclear magnetic dipole hyperfine interaction constants were taken from Lurio and Landmar [30] ($A(^{207}Pb(6^3P_2))$ = 2580 MHz (86.1 millikaysers)) and Saloman and Harper [23] ($A(^{207}Pb(7^3P_1))$ = 8811 MHz (294 millikaysers)). The relative intensities for the hyperfine components were obtained using the standard angular momentum relationships [31]. Details of Voigt profile calculations can be found elsewhere [9, 15]. Extensive discussion of the relative contributions of Lorentz and Doppler widths are not justified because the line shapes presented here are only examples to illustrate large effects (see later). We employ an arbitrary Voigt profile parameter [15] α = 0.117 (from an arbitrary Lorentz width) which yields, in the case of the transition at λ = 283.31 nm, a line shape similar to that reported by Cross and Husain [6] who, incidentally, used $A(^{207}(Pb(7^3P_1)))$ = 8813 MHz following Kopferman [32]. Integrals for the Voigt profiles were computed using the fast subroutine of Sundius [33] (normalized for a lorentzian distribution) which will generate small spikes in the profiles for low values of α. This is a minor artefact of the computer program [11], and the spikes were removed in Fig. 3.

We presented detailed calculations using various models for radiation trapping in our previous paper on Bi($6^4S_{3/2}$) [11] and demonstrated that the Holstein–Walsh (HW) model [34 - 36], which is in good agreement with the Kenty model [37 - 40] across a large atomic density range and which employs a maxwellian distribution in both the emitting and absorbing atoms, is much more convenient from the computational point of view. The ratio of the effective lifetime τ^* to the true radiative lifetime τ was calculated for Pb(6^3P_0) (λ = 283.31 nm), Pb(6^3P_2) (λ = 405.78 nm) and, for comparison with earlier work, Bi($6^4S_{3/2}$) (λ = 306.77 nm, (Bi($7^4P_{1/2}$) → Bi($6^4S_{3/2}$))) across a wide density range of the lower state and an arbitrary Lorentz width $\Delta\bar{\nu}_L$ such that α = 0.117 in all three cases. For atomic densities below 10^{13} atoms cm^{-3}, we employ the Samson–Milne–Blickensderfer (SMB) model [11, 41 - 43] for the solution of the diffusion equation for radiation [15]. For densities of 10^{14} atoms cm^{-3}, the HW model [11, 34 - 36] is used. The

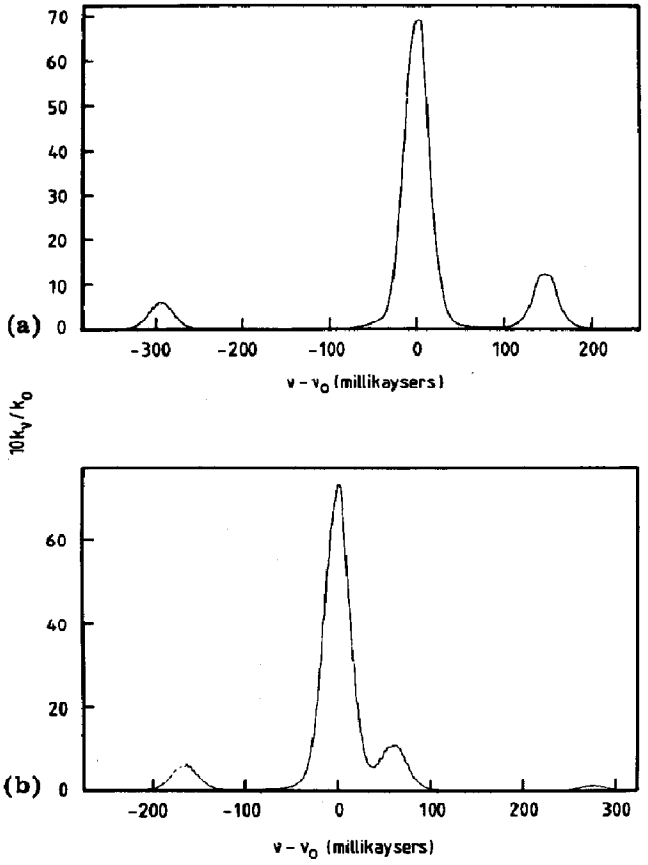

Fig. 3. Computer simulation of the line shapes of the atomic transitions at (a) $\lambda = 283.31$ nm ($Pb(7^3P_1) \rightarrow Pb(6^3P_0)$) and (b) $\lambda = 405.78$ nm ($Pb(7^3P_1) \rightarrow Pb(6^3P_2)$) obtained by summing the Voigt profiles over the transitions associated with the nuclear hyperfine components ($T = 298$ K; Voigt profile parameter $\alpha = 0.117$; components measured from line centres taken as exactly $\lambda = 283.31$ nm and $\lambda = 405.78$ nm; 21.1% ^{207}Pb ($I = 1/2$); 78.9% ^{204}Pb, ^{206}Pb and ^{208}Pb ($I = 0$).

(a)		*(b)*	
Position (millikaysers)	*Relative intensity*	*Position* (millikaysers)	*Relative intensity*
−294	0.070	−165	0.0704
0	0.789	0	0.789
147	0.141	60.9	0.1266
		276	0.0140

results are shown in Table 1. We can conclude that, for a given atomic density, radiation trapping effects are much larger for $Pb(6^3P_0)$ and $Pb(6^3P_2)$ than for $Bi(6^4S_{3/2})$. This arises primarily because there is no significant light absorption at the line centre of the atomic bismuth transition [11] at the helium pressure (about 4 kPa) used, in contrast with the line shapes of atomic lead (Fig. 3). However, because the population of $Pb(6^3P_2)$ is close

TABLE 1

Variation of τ^*/τ for fluorescence transitions of atomic lead and bismuth as a function of atomic density for a cylinder of radius R 1 cm

	τ^*/τ				$\Delta\bar{\nu}_D$ (milli-kaysers)	$\Delta\bar{\nu}_L$ (milli-kaysers)
	10^{11} atoms cm^{-2}	10^{12} atoms cm^{-2}	10^{13} atoms cm^{-2}	10^{14} atoms cm^{-2}		
$Pb(6^3P_0)$	1.17	2.80	9.31	157	30.3	3.35
$Pb(6^3P_2)$	1.21	3.18	10.1	92.1	21.1	2.06
$Bi(6^4S_{3/2})$	1.05	1.51	6.56	17.2	27.9	3.00

T = 298 K; α = 0.117.

to zero in these experiments (see later), radiation trapping will be negligible for these direct-line fluorescence measurements.

The expression for the fluorescence intensity detected radially from the axis of the resonance source is given by [44]

$$I_F = \frac{\Omega\Phi I_0 l}{4\pi \int_0^\infty k_{\nu'}\, d\nu'} \int_0^\infty \{1 - \exp(-k_\nu l)\}\, d\nu \int_0^\infty \{1 - \exp(-k_{\nu'} l)\}\, d\nu' \qquad (5)$$

where $\Phi = gA/\Sigma gA$ is the effective quantum yield for a particular atomic line ($\Phi_1(\lambda = 283.31\ nm) = 0.629$ and $\Phi_2(\lambda = 405.78\ nm) = 0.281$; also $\Phi_3(\lambda = 363.96\ nm) = 0.036$ for $Pb(7^3P_1) \rightarrow Pb(6^3P_1)$, which is not used in the present calculations). Ω is the solid angle subtended at the detector and l is the diameter of the cone of light from the resonance source. ν and ν' refer to the absorbing line and the emitting line respectively. In this calculation we need to consider (a) resonance fluorescence (λ = 283.31 nm) and (b) direct-line fluorescence (λ = 405.78 nm). For resonance fluorescence $\nu = \nu'$ (eqn. (5)); for direct-line fluorescence, eqn. (5) reduces to the simple form

$$I_F = \frac{\Omega\Phi I I_0}{4\pi} \int_0^\infty \{1 - \exp(-k_\nu l)\}\, d\nu \qquad (6)$$

This holds for no radiation trapping, *i.e.* $[Pb(6^3P_2)] = 0$, which is a good approximation as any $Pb(6^3P_2)$ generated by pulsed irradiation would have been rapidly quenched by collisions in the timescales involved here [45], and the population of this state by emission at λ = 405.78 nm is negligible.

The results of the calculations relating the fluorescence intensity and the particle density of $Pb(6^3P_0)$ are shown in Fig. 4. Clearly, as would be expected for densities as high as $[Pb(6^3P_0)] = 10^{14}$ atoms cm^{-3}, radiation trapping using the resonance transition would be very large. Direct-line fluorescence (λ = 405.78 nm) (Fig. 4) clearly avoids the effects of radiation trapping and results in an increase in the sensitivity for kinetic experiments.

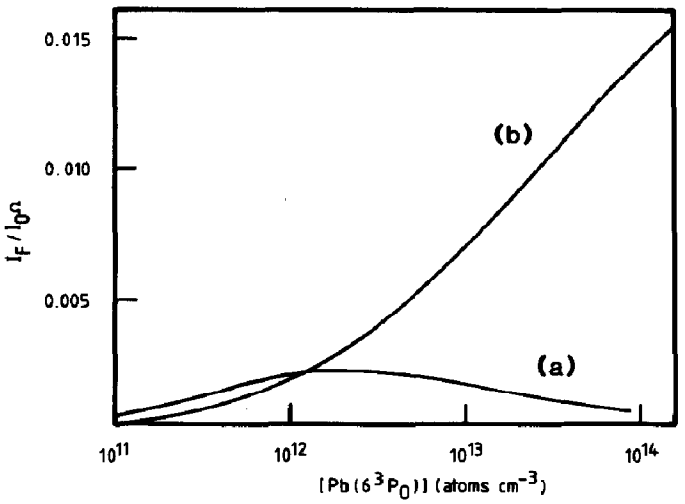

Fig. 4. Calculated intensity of fluorescence from a unit cell (l = 1 cm) as a function of the ground state atomic lead concentration in terms of the intensity I_0 of the resonance line at λ = 283.31 nm (Pb(7^3P_1) → Pb(6^3P_0)) for a continuum source subtending a solid angle Ω at the detector (Voigt profile parameter α = 0.117): curve a, resonance fluorescence at λ = 283.31 nm; curve b, fluorescence at λ = 405.78 nm (Pb(7^3P_1) → Pb(6^3P_2)).

This is a major factor facilitating the present time-resolved measurements at this wavelength for kinetic studies of Pb(6^3P_0).

3.3. *Kinetics of Pb(6^3P_0)*

Figure 5 gives examples of the time variation of the direct-line fluorescence I_F at λ = 405.78 nm (Pb(7^3P_1) → Pb(6^3P_2)) and shows the decay of Pb(6^3P_0) following optical excitation via the resonance transition at λ = 283.31 nm (Pb(7^3P_1) ← Pb(6^3P_0)) subsequent to the pulsed irradiation of $Pb(CH_3)_4$ in the presence of excess helium and molecular oxygen. We have shown in similar measurements in the kinetic study of Bi($6^4S_{3/2}$) by time-resolved resonance fluorescence [9 - 11] that the fluorescence intensity can be described by

$$I_F = \theta_1 + \theta_2 \exp(-k't) \tag{7}$$

where k' is the first-order decay coefficient for Pb(6^3P_0) in these measurements and is the prime object of kinetic interest. The computerized fitting of the digitized output according to eqn. (7) is also shown in Fig. 5. θ_1 is included to take account of the steady scattered light signal (λ = 405.78 nm) from the resonance source. It is immediately apparent from a visual inspection of Fig. 5 that the particularly low value of I_F at longer times, *i.e.* θ_1/θ_2, is much smaller (by at least a factor of 10) than the values typically encountered when employing a resonance transition [9 - 11]. The time-dependent fluorescence intensity due to the decay of Pb(6^3P_0) can be identified with the second term on the right-hand side of eqn. (7) and expressed, following a kinetic analysis similar to that described for other atoms [8], by

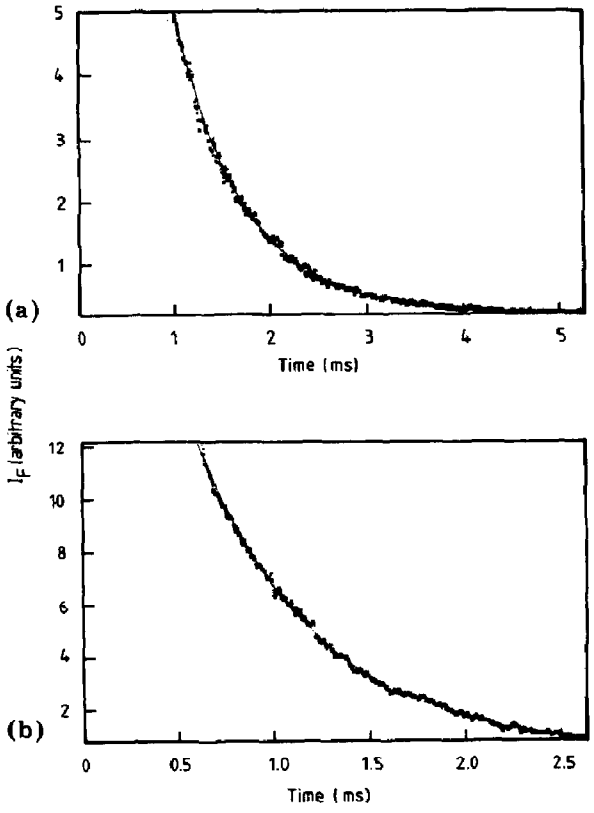

Fig. 5. Digitized time variation of the atomic emission intensity I_F at $\lambda = 405.8$ nm ($Pb(7s(^3P_1^\circ)) \rightarrow Pb(6p^2(^3P_2))$) showing the decay of ground state lead atoms $Pb(6^3P_0)$ following optical excitation at $\lambda = 283.3$ nm ($Pb(7s(^3P_1^\circ)) \leftarrow Pb(6p^2(^3P_0))$) subsequent to the pulsed irradiation of $Pb(CH_3)_4$ in the presence of oxygen and excess helium using a high intensity Garton–Wheaton flash lamp ($E = 500$ J; $[Pb(CH_3)_4] = 5.2 \times 10^{14}$ molecules cm^{-3}; $[He] = 9.0 \times 10^{17}$ atoms cm^{-3}) (×, data points; ——, computerized curve fitting to $I_F = \theta_1 + \theta_2 \exp(-k't)$): (a) $[O_2] = 0$; (b) $[O_2] = 3.7 \times 10^{16}$ molecules cm^{-3}.

$$I_F(t) = \frac{\phi\{Pb(6^3P_0)\}_{t=0} \exp(-k't)}{1 + \Sigma k_Q[Q]_i/gk_f} \tag{8}$$

where gk_f is the effective fluorescence decay rate with no quenching gas present. Without radiation trapping $gk_f = 1/\tau_e$, and with radiation trapping $gk_f < 1/\tau_e$. $\Sigma k_Q[Q]_i$ is the first-order kinetic contribution to the fluorescence quenching of $Pb(7^3P_1)$. ϕ combines all the terms involved in optical excitation by the resonance source at $\lambda = 283.31$ nm ($Pb(7^3P_1) \leftarrow Pb(6^3P_0)$) together with the efficiency of light collection and electronic amplification of the photoelectric signals.

The observed fluorescence signals (Fig. 5) were analysed by computer using the LAMFIT procedure of Powell [46] to estimate a value for θ_1 as this quantity is independent of the units of time employed. The full curves in Fig. 5 show the effect of curve fitting of the digitized decay traces using

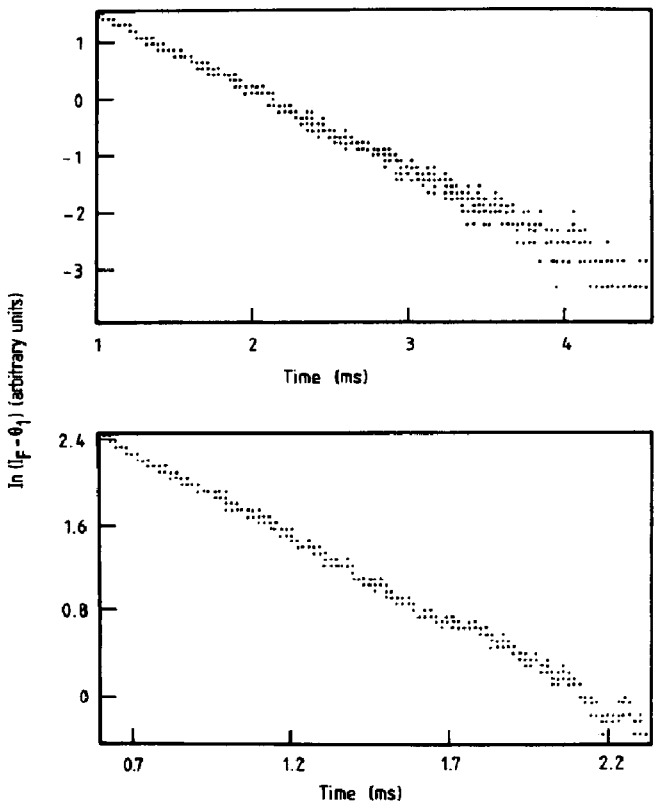

Fig. 6. Computerized output of the digitized first-order kinetic plots derived from time-resolved atomic emission I_F at λ = 405.8 nm ($Pb(7^3P_1^\circ) \rightarrow Pb(6^3P_2)$) showing the removal of ground state lead atoms $Pb(6^3P_0)$ following optical excitation at λ = 283.3 nm ($Pb(7^3P_1^\circ) \leftarrow Pb(6^3P_0)$) subsequent to the pulsed irradiation of $Pb(CH_3)_4$ in the presence of oxygen and excess helium using a high intensity Garton–Wheaton flash lamp (E = 500 J; $[Pb(CH_3)_4] = 5.2 \times 10^{14}$ molecules cm^{-3}; $[He] = 9.0 \times 10^{17}$ atoms cm^{-3}) (●, data points; computerized fitting to the form $\ln(I_F - \theta_1)$ *vs.* t): (a) $[O_2] = 0$; (b) $[O_2] = 3.7 \times 10^{16}$ molecules cm^{-3}.

this procedure. The effect of the low value of θ_1 is seen in the quality of the first-order kinetic plots constructed from data of the type shown in Fig. 5. Hence plots of $\ln(I_F - \theta_1)$ *versus* t are presented in Fig. 6 from the data of Fig. 5 yielding the values of k' from the slopes. There is normally greater scatter in such first-order kinetic plots at long times [10].

A kinetic limitation of the present system is the need to employ $Pb(CH_3)_4$ at relatively high concentrations as indicated in Figs. 5 and 6 in order to obtain fluorescence signals at λ = 405.78 nm. Whilst the variation of k' with $[Pb(CH_3)_4]$ across the range from about 10^{14} to 10^{15} molecules cm^{-3} is scattered, the data indicate an effective second-order rate constant $k_2(Pb(6^3P_0) + Pb(CH_3)_4)$ of $(1.0 \pm 0.4) \times 10^{-13}$ cm^3 molecules^{-1} s^{-1} at 300 K. Determination of the true value would require a detailed knowledge of the extent of photolysis. Reproducibility is difficult to sustain, particularly

because of the low wavelength transmission of the LiF window coupling the source to the reactor. Hence only an approximately linear relationship between θ_2 and $[Pb(CH_3)_4]_{initial}$, and hence presumably $[Pb(6^3P_0)]_{t=0}$ (eqn. (8)), was observed across the same concentration range of $Pb(CH_3)_4$ (see above). Nevertheless we have succeeded in obtaining time-resolved atomic fluorescence measurements on $Pb(6^3P_0)$ and in extracting kinetic data. This principally concerns the third-order reactions between lead, oxygen and helium and between lead, NO and helium which have hitherto been studied by time-resolved resonance absorption spectroscopy [1 - 3]. These third-order processes are investigated with the necessary accompanying effects of diffusion resulting from the variation of p_{He} and the removal of $Pb(6^3P_0)$ by the photochemical precursor $Pb(CH_3)_4$. Hence kinetic removal of $Pb(6^3P_0)$ in the presence of oxygen, for example, can be expressed in the form

$$-\frac{d[\ln\{[Pb(6^3P_0)]\}]}{dt} = k' = K + \frac{\beta}{p_{He}} + k_3[O_2][He] \quad (9)$$

and similarly for NO. K primarily represents removal by $Pb(CH_3)_4$ ($K = k_2[Pb(CH_3)_4] \equiv k_R$). k', corrected for the first-order contribution by K, can thus be expressed in the form

$$\frac{k'(\text{corrected})}{p_{He}} = k_3[O_2] + \frac{\beta}{p_{He}^2} \quad (10)$$

Figure 7 summarizes the data for the third-order reactions between lead, oxygen and helium and between lead, NO and helium, accompanied by diffusion, plotted in the form of eqn. (10). The slopes of these plots yield empirical diffusion coefficients β for $Pb(6^3P_0)$ in helium of 3.7×10^6 Pa s^{-1} and 4.4×10^6 Pa s^{-1} from Figs. 7(a) and 7(b) respectively, and are in reasonable accord. Unfortunately the boundary conditions of the effective reaction volume required to yield genuine diffusion coefficients are not well defined; however, if we employ the "long-time" solution to the diffusion equation for a cylinder [15, 47]

$$\beta = \left(\frac{\pi^2}{l^2} + \frac{5.81}{r^2}\right) D_{12} \quad (11)$$

and the approximations $l = 1$ cm and $r = 0.5$ cm, we obtain $D_{12}(Pb(6^3P_0)$–$He) = 0.9 \pm 0.3$ cm^2 s^{-1} at 1 atm, which is a reasonable value (*i.e.* within a factor of 2) for this type of quantity. However, β is used empirically in these experiments for the purpose of analysing the kinetic data. Its value is much larger than that found in the analogous measurements on $Bi(6^4S_{3/2})$ [9 - 11]. The rate of removal of $Pb(6^3P_0)$ by diffusion was a serious limiting kinetic factor in these experiments.

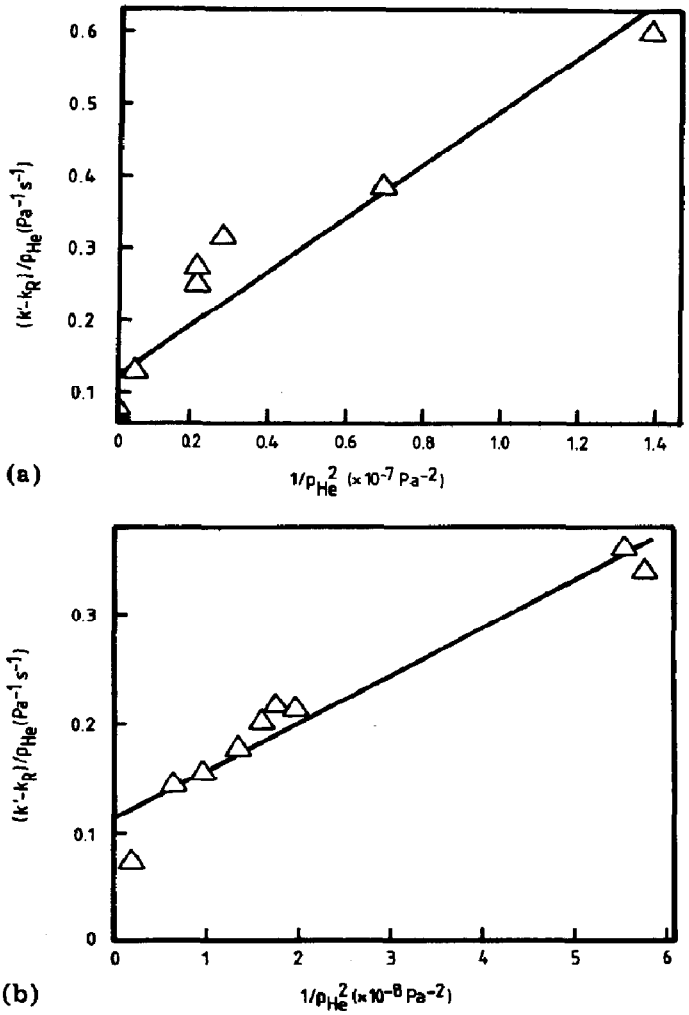

Fig. 7. Variation of the pseudo-first-order rate coefficient for the decay of $Pb(6^3P_0)$ in the presence of oxygen, and NO and excess helium ($(k' - k_R)/p_{He}$ *vs.* $1/p_{He}^2$), indicating the effects of both third-order kinetics and diffusion. (a) $[O_2] = 9.9 \times 10^{15}$ molecules cm^{-3}, $[Pb(CH_3)_4] = 1.6 \times 10^{15}$ molecules cm^{-3}; (b) $[NO] = 3.8 \times 10^{14}$ molecules cm^{-3}, $[Pb(CH_3)_4] = 2.0 \times 10^{14}$ molecules cm^{-3}.

The intercepts of Figs. 7(a) and 7(b), coupled with the concentrations of oxygen and NO, yield $k_3(Pb + O_2 + He) \approx 4 \times 10^{-32}$ cm^6 molecules^{-2} s^{-1} (300 K) and $k_3(Pb + NO + He) \approx 1 \times 10^{-30}$ cm^6 molecules^{-2} s^{-1} (300 K). For reasons indicated above, the relatively rapid rate of reaction between lead and the NO–He mixture prevents investigation of this rate process across a significant concentration range of NO for reasonable pressures of helium required in measurements of the present type and hence the intercept in Fig. 7(b) yields, at present, the only measurement of $k_3(Pb + NO + He)$ by time-resolved atomic fluorescence. The value quoted for this rate constant in Table 2 represents the average of the results of four such plots.

TABLE 2

Comparison of k_3(Pb + O_2 + He) and k_3(Pb + NO + He) from time-resolved atomic fluorescence and time-resolved atomic resonance absorption measurements

Technique	k_3(Pb + O_2 + He)	k_3(Pb + NO + He)
Fluorescence	$(2.5 \pm 0.2) \times 10^{-32}$ (this work)	$(9 \pm 3) \times 10^{-31}$ (this work)
Absorption	$(1.4 \pm 1.0) \times 10^{-32}$ [3]	$\approx 2 \times 10^{-30}$ [3]
Absorption	7×10^{-33} [2]	$\approx 2.6 \times 10^{-30}$ [1]

T = 300 K; error, 2σ.
k_3, cm^6 molecule^{-2} s^{-1}.

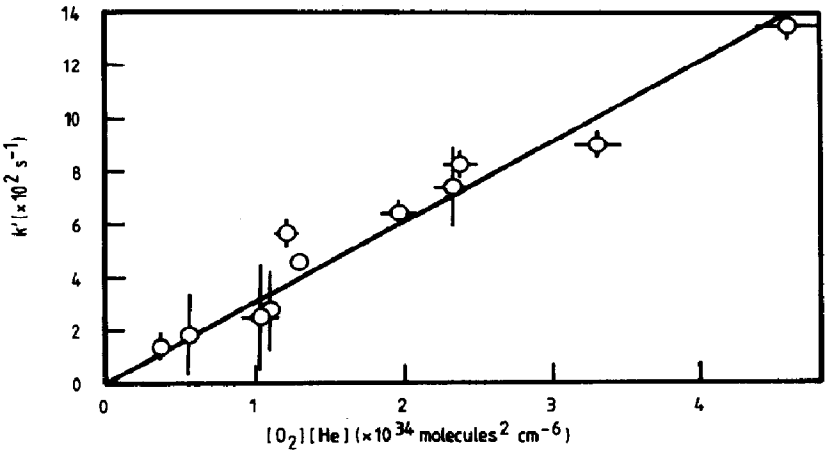

Fig. 8. Variation of the pseudo-first-order rate coefficient k' (diffusion corrected and normalized) for the decay of Pb(6^3P_0) in the presence of oxygen and helium (E = 500 J; [$Pb(CH_3)_4$] = 6×10^{14} molecules cm^{-3}).

A limited number of decay measurements could be made by varying the concentration of oxygen. Figure 8 shows the first-order decay coefficients corrected for both the contribution of $k_R(Pb(CH_3)_4)$ and β/p_{He} given quantitatively above plotted against [O_2][He] and constrained to pass through the origin. This yields k_3(Pb + O_2 + He) = $(2.5 \pm 0.2) \times 10^{-32}$ cm^6 molecules^{-2} s^{-1} (300 K), which is the value we report (Table 2).

The results of the present investigation can be compared with the data reported for these third-order reactions derived from time-resolved resonance absorption measurements. These are given in Table 2. There is reasonable agreement between the present result for k_3(Pb + O_2 + He) and the more recent value derived from resonance absorption measurements by Cross and Husain [3], particularly bearing in mind that a γ value of 0.38 ± 0.04 was employed for the transition at λ = 283.31 nm in the analysis of these measurements. The time-resolved resonance absorption data for k_3(Pb + NO + He) [1, 3] are only reported as estimates.

Finally, the present data can be used to estimate fluorescence quenching cross sections for Pb(7^3P_1). We have shown [9] that measure-

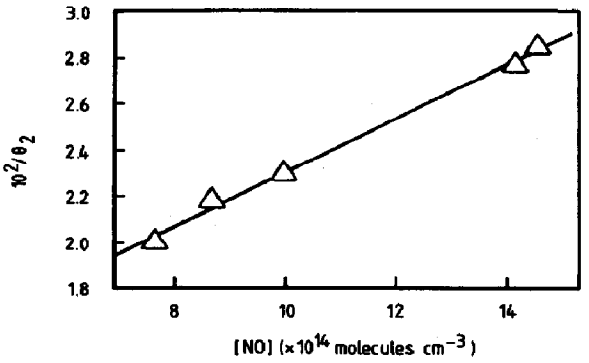

Fig. 9. Stern–Volmer plot ($1/\theta_2$ *vs.* [Q]) for the collisional quenching of $Pb(7^3P_1)$ by NO obtained by time-resolved atomic emission at λ = 405.8 nm ($Pb(7^3P_1) \rightarrow Pb(6^3P_2)$) following optical excitation at λ = 283.3 nm ($Pb(7^3P_1) \leftarrow Pb(6^3P_0)$) subsequent to the generation of $Pb(6^3P_0)$ by pulsed irradiation of $Pb(CH_3)_4$ (E = 500 J; $[Pb(CH_3)_4] = 5 \times 10^{14}$ molecules cm^{-3}; $[He] = 8 \times 10^{17}$ atoms cm^{-3}).

ments of θ_2 from the curve-fitting procedure on eqn. (7) [46] coupled with eqn. (8) can be used to construct Stern–Volmer plots. Hence, for example, a set of measurements can be carried out in which θ_2 is determined for various values of [NO] with a given $Pb(CH_3)_4$–He mixture. Such a plot, *i.e.* $1/\theta_2$ *versus* [Q], is illustrated in Fig. 9 for a limited body of data for NO. These are particularly difficult measurements to make in this type of system as θ_2 is much more sensitive to photochemical reproducibility (see above) than is k'. Figure 9 yields the fluorescence quenching cross section $\sigma_{NO}^2 = 38 \pm 3$ Å^2. The data for the variation of θ_2 with $[O_2]$ were obtained over a wider range than that indicated for NO in Fig. 9 and were more scattered but nevertheless permitted an estimate of the quenching cross section with this molecule, *i.e.* $\sigma_{O_2}^2 = 12 \pm 8$ Å^2. This can be compared with the value of $\sigma_{O_2}^2 = 15 \pm 3$ Å^2 obtained by Jenkins [48] from flame investigations (1400 K).

Acknowledgments

We thank Dr. J. R. Grove of the Associated Octel Company for a sample of lead tetramethyl. We are again indebted to Mr. C. J. Smith of the glass blowing department of the laboratory for the careful construction of the sealed capsules used in the microwave-powered atomic emission source.

References

1 D. Husain and J. G. F. Littler, *J. Photochem.*, *2* (1974) 247.
2 D. Husain and J. G. F. Littler, *Combust. Flame*, *22* (1974) 295.
3 P. J. Cross and D. Husain, *J. Photochem.*, *7* (1977) 157.
4 P. J. Cross and D. Husain, *J. Photochem.*, *8* (1978) 183.
5 P. J. Cross and D. Husain, *J. Photochem.*, *9* (1978) 369.
6 P. J. Cross and D. Husain, *J. Photochem.*, *10* (1979) 251.
7 D. Husain and N. K. H. Slater, *J. Photochem.*, *6* (1977) 325.

8 D. Husain, L. Krause and N. K. H. Slater, *J. Chem. Soc., Faraday Trans. II, 73* (1977) 1678.
9 C. F. Bell and D. Husain, *J. Photochem., 24* (1984) 207.
10 C. F. Bell and D. Husain, *J. Photochem., 24* (1984) 223.
11 C. F. Bell and D. Husain, *J. Photochem., 26* (1984) 229.
12 D. Husain, *Ber. Bunsenges. Phys. Chem., 81* (1977) 168.
13 D. Husain and N. K. H. Slater, *J. Chem. Soc., Faraday Trans. II, 76* (1980) 606.
14 R. J. Donovan, D. Husain and L. J. Kirsch, *Trans. Faraday Soc., 66* (1970) 2551.
15 A. C. G. Mitchell and M. W. Zemansky, *Resonance Radiation and Excited Atoms*, Cambridge University Press, Cambridge, 1971, p. 246.
16 P. J. Cross and D. Husain, *J. Photochem., 10* (1979) 297.
17 W. R. S. Garton, *J. Sci. Instrum., 36* (1959) 11.
18 C. I. M. Beenakker, *Spectrochim. Acta, Part B, 31* (1976) 483.
19 C. I. M. Beenakker, *Spectrochim. Acta, Part B, 32* (1977) 173.
20 C. I. M. Beenakker and P. J. W. M. Boumans, *Spectrochim. Acta, Part B, 33* (1978) 53.
21 D. Husain, L. Krause and N. K. H. Slater, *J. Chem. Soc., Faraday Trans. II, 73* (1977) 1706.
22 C. E. Moore (ed.), *Atomic Energy Levels, NBS Natl. Stand. Ref. Data Ser. 35*, 1971 (National Bureau of Standards, U.S. Department of Commerce).
23 E. B. Saloman and W. Harper, *Phys. Rev., 7* (1966) 144.
24 P. T. Cunningham and J. K. Link, *J. Opt. Soc. Am., 47* (1967) 1000.
25 D. Husain and J. Schifino, *J. Chem. Soc., Faraday Trans. II, 78* (1982) 2083.
26 A. U. Acuna, D. Husain and J. R. Wiesenfeld, *J. Chem. Phys., 58* (1973) 494.
27 E. W. Abel, in J. C. Bailar, H. J. Emeleus, R. Nyholm and A. F. Trotman-Dickenson (eds.), *Comprehensive Inorganic Chemistry*, Vol. 2, Pergamon, Oxford, 1973, p. 105.
28 M. I. Christie and G. Porter, *Proc. R. Soc. London, Ser. A, 212* (1952) 398.
29 W. Gordy, W. A. Smith and R. F. Trambarulo, *Microwave Spectroscopy*, Dover Publications, New York, 1960, p. 436.
30 A. Lurio and D. A. Landmar, *J. Opt. Soc. Am., 60* (1970) 759.
31 H. E. White and A. Y. Eliason, *Phys. Rev., 44* (1933) 753.
32 H. Kopferman, *Z. Phys., 75* (1932) 363.
33 T. Sundius, *J. Raman Spectrosc., 1* (1973) 417.
34 T. Holstein, *Phys. Rev., 72* (1947) 1212.
35 T. Holstein, *Phys. Rev., 83* (1951) 1159.
36 P. J. Walsh, *Phys. Rev., 116* (1959) 511.
37 C. Kenty, *Phys. Rev., 31* (1928) 997.
38 C. Kenty, *Phys. Rev., 42* (1932) 823.
39 M. Zemansky, *Phys. Rev., 29* (1927) 513.
40 M. Zemansky, *Phys. Rev., 42* (1932) 843.
41 E. W. Samson, *Phys. Rev., 40* (1932) 940.
42 E. A. Milne, *J. London Math. Soc., 1* (1926) 40.
43 R. P. Blickensderfer, W. H. Breckenridge and J. Simons, *J. Chem. Phys., 80* (1976) 653.
44 G. F. Kirkbright and M. Sargent, *Atomic Absorption and Fluorescence Spectroscopy*, Academic Press, New York, 1974.
45 D. Husain and J. G. F. Littler, *Int. J. Chem. Kinet., 6* (1974) 61.
46 M. J. D. Powell, personal communication, 1979; cited in D. Husain and N. K. H. Slater, *J. Chem. Soc., Faraday Trans. II, 76* (1980) 606.
47 M. W. Zemansky, *Phys. Rev., 34* (1929) 213.
48 D. R. Jenkins, *Proc. R. Soc. London, Ser. A, 313* (1969) 551.